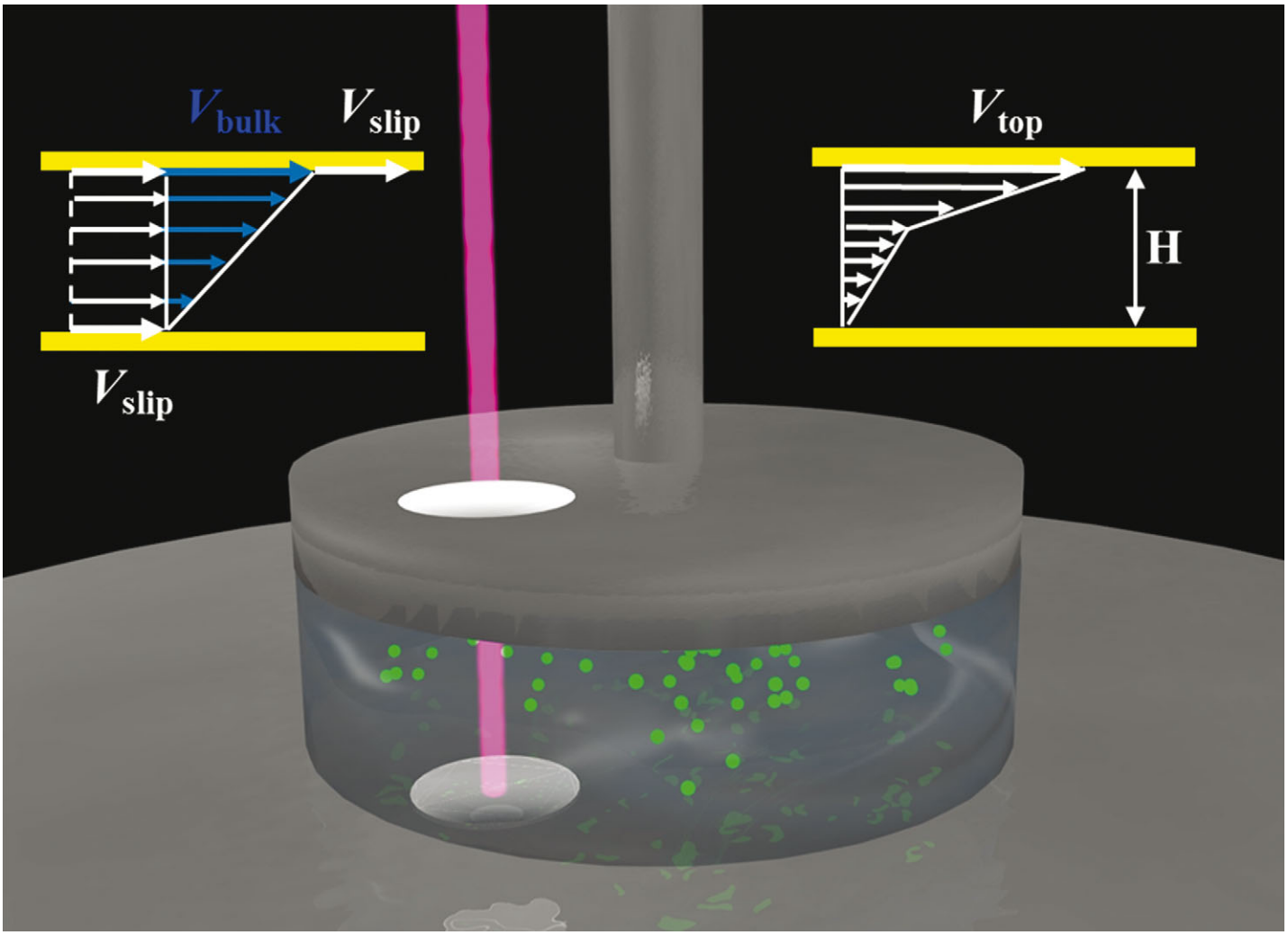

Highlighting research results from the Department of Chemical Engineering at Delft University of Technology (The Netherlands).

Shear banding in entangled polymers in the micron scale gap: a confocal-rheoscopic study

In this work, we experimentally elucidate how molecular parameters such as slip length influence the shear inhomogeneity of entangled liquids during shear in a small gap. By reducing the slip length of a solution, wall slip can be replaced by bulk shear banding during shear.

As featured in:

See Pouyan E. Boukany *et al.*, *Soft Matter*, 2015, **11**, 8058.

ROYAL SOCIETY OF CHEMISTRY

www.softmatter.org

Registered charity number: 207890

Soft Matter

PAPER

View Article Online
View Journal | View Issue

Cite this: *Soft Matter*, 2015, **11**, 8058

Shear banding in entangled polymers in the micron scale gap: a confocal-rheoscopic study

Pouyan E. Boukany,*[a] Shi-Qing Wang,[b] Sham Ravindranath[b] and L. James Lee[c]

Received 9th June 2015,
Accepted 8th September 2015

DOI: 10.1039/c5sm01429h

www.rsc.org/softmatter

Recent shear experiments in well-entangled polymer solutions demonstrated that interfacial wall slip is the only source of shear rate loss and there is no evidence of shear banding in the micron scale gap. In this work, we experimentally elucidate how molecular parameters such as slip length, b, influence shear inhomogeneity of entangled polybutadiene (PBD) solutions during shear in a small gap $H \sim 50$ μm. Simultaneous rheometric and velocimetric measurements are performed on two PBD solutions with the same level of entanglements ($Z = 54$) in two PBD solvents with molecular weights of 1.5 kg mol^{-1} and 10 kg mol^{-1} that possess different levels of shear inhomogeneity ($2b_{max}/H = 17$ and 240). For the PBD solution made with a low molecular weight PBD solvent of 1.5 kg mol^{-1}, wall slip is the dominant response within the accessible range of the shear rate, *i.e.*, up to the nominal Weissenberg number (Wi) as high as 290. On the other hand, wall slip is minimized using a high molecular-weight PBD solvent of 10 kg mol^{-1} so that bulk shear banding is observed to take place in the steady state for Wi > 100. Finally, these findings and previous results are in good agreement with our recently proposed phase diagram in the parameter space of apparent Wi *versus* $2b_{max}/H$ suggesting that shear banding develops across the micron scale gap when the imposed Wi exceeds $2b_{max}/H$ [Wang *et al.*, *Macromolecules*, 2011, **44**, 183].

1 Introduction

Polymeric materials including DNA, actin filaments, plastics, textiles, rubbers and elastomers have emerged as a prominent class of soft matter, which can be found everywhere in nature and industry.[1] Long macromolecules can be entangled in their disordered liquid state and display remarkable viscoelastic properties.[2,3] Their sluggish macroscopic relaxation arises from chain uncrossability that constrains chains to perform "reptation"[4] in the curvilinear one directional tube in quiescence.[5,6] Under large fast deformation (when the deformation rate exceeds the reciprocal of the reptation time), the intertwining chains pull on each other, resulting in molecular deformation, until the point of force imbalance, leading to chain disentanglement and yielding of the entanglement network.[7] Whether chain disentanglement during large deformation produces a uniform shear field or not is a key issue in the nonlinear rheology of polymers.

Experimental knowledge about nonlinear rheological behavior of entangled polymers typically derives from a rotational shear rheometer where the sample thickness, H, is in the range of 1 mm. Recent experiments combined traditional rheometric measurements with particle-tracking velocimetric (PTV) characterization to obtain more insightful information about how chain entanglement responds to startup shear. At a high Weissenberg number Wi $= \dot{\gamma}\tau > 1$, defined as the product of the bulk shear rate $\dot{\gamma}$ and the longest relaxation (or reptation) time τ, many entangled fluids exhibit wall slip and shear banding, including wormlike micelles,[8–12] polybutadiene (PBD),[13–15] polyacrylamide,[16,17] DNA,[18–20] and F-actin solutions,[21] as well as polymer melts such as styrene-butadiene[22] and polyethylene-oxide.[23] On the other hand, such shear banding can be avoided by replacing the sudden startup with gradual ramping up of the applied shear rate.[24,25] Moreover, shear banding and wall slip need not occur when the system is insufficiently entangled (the level of entanglements per chain $Z < 40$)[14,26,27] or has a negligibly small extrapolation length b relative to the sample thickness H, *i.e.*, when $b/H \ll 1$.[14,28,29]

Recent velocimetric measurements based on the confocal microscopy asserted that there was no bulk shear banding in entangled PBD solutions when the gap of the shear cell is reduced to tens of microns:[30,31] Wall slip was the only discernible form of shear inhomogeneity, with linear velocity profiles across the gap for a high level of entanglement, *i.e.*, $Z = 56$ entanglements per chain. Such results were used to suggest that the previously observed shear banding[13,14] involving a conventional cone-plate

[a] *Department of Chemical Engineering, Delft University of Technology, Julianalaan 136, 2628 BL Delft, The Netherland. E-mail: P.E.Boukany@tudelft.nl; Tel: +31-(0)15-27 89981*
[b] *Department of Polymer Science and Maurice Morton, Institute of Polymer Science, University of Akron, Akron, Ohio 44325, USA*
[c] *Department of Chemical and Biomolecular Engineering, The Ohio State University, 174 West 18th Avenue, Columbus, Ohio 43210, USA*

or a parallel-disk device was due to the edge fracture: the absence of shear banding in a shear cell with a gap distance much lower than the conventional gap (*e.g.*, by a factor of 20) was assumed to be due to the fact that there is a negligible effect of edge fracture in the shear cell with a 50 μm gap.

Wall slip is a well-established phenomenon in both polymer melts and solutions.[32] During startup shear with Wi > 1, entangled polymers show the first sign of shear inhomogeneity in the form of wall slip by interfacial disentanglement, because the polymer/wall interface is weaker than the cohesion of entangled networks.[33] The intrinsic ability of the entangled solution to undergo slip can be estimated in terms of the slip length b. The magnitude of $b \sim (\eta/\eta_i)a$ relative to the sample thickness H determines how much the actual bulk shear rate $\dot{\gamma}_b$ is reduced from the nominal rate $\dot{\gamma}$,[19,29] where a is the interfacial layer thickness, η and η_i are the bulk and interfacial viscosities respectively. The maximum value of b, denoted as b_{max}, corresponds to the full interfacial disentanglement when η_i reduces to the solvent viscosity η_s, *i.e.*, $b_{max} = (\eta/\eta_s)a(\phi)$. For polymer solutions, a would grow from its value in the melt l_{ent} upon dilution as: $a(\phi) = l_{ent}\phi^{-0.66}$, where ϕ is the polymer volume fraction.

Upon startup shear with Wi > 1, wall slip will emerge as a consequence of interfacial yielding.[29,33] Denoting the effective shear rate in the bulk as $\dot{\gamma}_b$, then the speed of the shearing wall is given in terms of the slip velocity V_s as

$$V = \dot{\gamma}_b H + 2V_s, \tag{1a}$$

which can be rewritten as

$$\dot{\gamma} = (1 + 2b/H)\dot{\gamma}_b, \tag{1b}$$

where the nominal rate $\dot{\gamma} = V/H$ and the slip length b has its kinematic meaning according to $b = V_s/\dot{\gamma}_b$, which is illustrated in Fig. 1. With increasing V or $\dot{\gamma}$, V_s and b grow towards their maximum values. Before the maximum slip velocity is reached, the bulk shear rate $\dot{\gamma}_b$ can be expected to remain at a critically low value around $1/\tau$. Correspondingly, the steady-shear stress does not appreciably increase with $\dot{\gamma}$. In other words, the value of $\dot{\gamma}$ can increase up to $\dot{\gamma}_{wb\text{-}bnl} = (1 + 2b_{max}/H)/\tau$ without forcing the bulk to leave the Newtonian regime whose upper-bound is given as $1/\tau$.

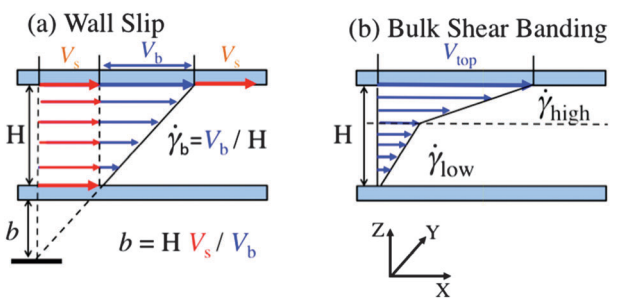

Fig. 1 Schematic diagram of the velocity profile within the gap of the shear geometry in the presence of (left) wall slip, where $b = V_s/\dot{\gamma}_b$, and (right) bulk shear banding at the apparent shear rate.

In other words, there is a critical Weissenberg number $Wi_{ws\text{-}bnl}$, beyond which the bulk starts to enter the nonlinear response regime, given by

$$Wi_{ws\text{-}bnl} = (1 + 2b_{max}/H) \tag{2}$$

When $Wi > Wi_{ws\text{-}bnl}$, even maximum wall slip cannot save the bulk from having $Wi_b = \dot{\gamma}_b\tau > 1$. Here the subscript "ws-bnl" stands for a transition from wall slip (ws) to bulk nonlinear response (bnl). For well-entangled polymer solutions, $Wi_{ws\text{-}bnl}$ can be very large when H is reduced from a conventional gap distance of 1 mm to 50 μm. This is a reason why Hayes *et al.* only reported wall slip as the source of shear rate loss for entangled PBD solutions.[30]

In passing, we also note that the maximum value of b_{max} corresponds to the slip velocity V_s attaining its maximum at $Wi_{ws\text{-}bnl}$ where the bulk shear rate $\dot{\gamma}_b \sim \tau^{-1}$. Thus, we have

$$V_{s(max)} = b_{max}/\dot{\gamma}_b \sim b_{max}/\tau \tag{3}$$

In the current study, we show that the dominant wall slip characteristic of the previous reports[30,31] is replaced by bulk shear banding when the extrapolation length b is reduced using a polymeric solvent of sufficient high molecular weight. Specifically, one of our two 13 wt% PBD solutions shows only wall slip, similar to one solution reported previously,[30,31] because of its high value for b_{max}, whereas the second solution displays bulk shear banding because of its lower value for b_{max}. Because the point of velocimetric observation in our setup is at least 3 mm away from the meniscus in a parallel-disk shear cell with $H \sim 50$ μm, the aspect ratio is 60, no edge fracture and sample loss took place during shear. Finally, our findings in the micron scale gap are presented in terms of a phase diagram in the parameter space of apparent Wi *versus* $2b_{max}/H$. We demonstrate that b_{max} is a key parameter for a fixed gap to control what type of velocity profile may occur for a given Wi and bulk shear banding can develop when the applied Wi exceeds $2b_{max}/H$. At sufficiently high Wi, the linear velocity profile is recovered across the gap.

2 Experimental

2.1. Materials and sample preparation

Our experiments are based on two well-entangled 1,4-polybutadiene (PBD) solutions made with the same parent high molecular weight PBD ($M_w \sim 10^6$ g mol^{-1}) at the same 13 wt% concentration in polymeric butadiene (PBD) "solvents" (with molecular weights of 1.5 kg mol^{-1} and 10 kg mol^{-1}). In this work, these two solutions are labelled as 1M(13%)1.5K and 1M(13%)10K. The molecular characteristics of parent polymers and solvents are listed in Table 1. The parent PBD was first dissolved in excess of toluene to which the PBD solvent was added and intimately mixed. For the particle tracking velocimetric (PTV) observations, fluorescein isothiocyanate (FITC) labelled fluorescent melamine micro-beads with a particle size of 1 μm (Sigma Aldrich, CAT no 90305) were dispersed in toluene and then added to the solution with the final loading

Table 1 Molecular characteristics of parent 1MPBD, and 1.5KPBD and 10KPBD solvents

Sample	M_n (g mol^{-1})	M_w (g mol^{-1})	M_w/M_n	η_s (Pa s)	Source
1MPBD	1.01×10^6	1.05×10^6	1.03	n/a	Akron
1.5KPBD	1500	Not provided	Not provided	0.7	Sigma-Aldrich Cat No. 200484
10KPBD	8900	10 500	1.02	14	Bridgestone

of the particles around 600–800 ppm. Most of the toluene was evaporated at room temperature under a hood for days, and the remaining was removed by applying vacuum until the residual toluene is less than 0.5%.

2.2. Rheometric and velocimetric measurements

In this work, we integrated a Bohlin-CVOR rheometer with a spin-disk confocal microscope to make the particle-tracking velocimetric (PVT) measurements at an unconventionally low gap distance of H = *ca.* 50 μm. The schematic representation of our confocal rheoscope is shown in Fig. 2 that involves an Olympus IX-81 inverted microscope. An EM-CCD camera (Hammamutsa) connected to the CFM was used to take two-dimensional (2D) movies in the XY plane through a piezo-mounted objective lens (60×, 1.4 NA). The field of view in our measurements is about 100 μm × 100 μm where the PTV observations are performed at a distance of 3 mm from the meniscus so that the aspect ratio of the distance from the edge to the gap distance is *ca.* 60 (for H = 50 μm). The lateral resolution, axial resolution, and optical slice thickness are 0.2, 0.5, and 1.34 μm, respectively. The camera and spinning disk were synchronized, and the entire system was controlled using VoxCell software from Visitech International.

A custom-made microscope stage was designed so that our rheometer (Bohlin CVOR) could integrate with the stage mounted onto a confocal fluorescence microscope (CFM) with three adjustable screws to ensure alignment. Initially, the adjustable platform allowed us to pre-align the rheometer on an optical table, on which the CFM was placed. The rotating shaft has a short length of 2 cm to ensure good parallelism of the rotating disc to the bottom plate. To verify the alignment, the upper disc was first raised 5 μm above the stationary bottom plate and then spun to detect any misalignment. This setup has been previously employed to accurately conduct molecular imaging of entangled DNA solutions on the micron scale,[34] correlating interfacial slip with conformations of DNA adsorbed at wall.

All startup shear measurements were performed at room temperature around 25 °C, based on parallel-disk geometry with a radius R = 10 mm and H = *ca.* 50 μm. Here all apparent shear rate values in the fluid sample are estimated as $\dot{\gamma} = \Omega R/H$, where Ω is the imposed angular velocity at R = 7 mm (at a radial distance of 3 mm from the edge). To determine the linear viscoelastic properties of these two entangled PBD solutions, small amplitude oscillatory shear (SAOS, strain amplitude $\dot{\gamma}$ = 5%) frequency sweep tests were conducted in a conventional parallel-plate shear cell with H = 1 mm. All startup shear tests were performed in the controlled rate mode at a narrow gap (H = *ca.* 50 μm) under the confocal microscope to capture the velocity profiles across the gap. The top and bottom plates were a glass slide (thickness 0.15–0.17 mm). The bottom plate was placed on the microscope stage, along with a circular plastic O-ring (inner radius 14 mm) to minimize meniscus instability and sample loss during high shear. The top moving and bottom stationary transparent plates were identified by scanning along the sample thickness direction to confirm that the nominal gap is consistent with the true gap. In all startup shear experiments, 2D images were captured every 2 to 4 microns across the sample thickness (with a rate of 35 to 45 fps) to measure both the transient and steady velocity profile across the gap. Typical error bars in the measured velocity are about 5%, which was achieved by keeping track of sufficiently large displacements of the fluorescent particles.

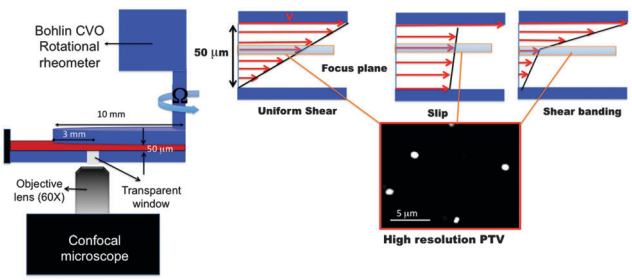

Fig. 2 (left) Schematic illustration of the rheo-confocal setup used for simultaneous rheometric and velocimetric measurements at room temperature with H = *ca.* 50 μm. (right) Sketch of the parallel-disk geometry with three different velocity profiles: uniform flow, slip and shear banding. The velocity profiles were measured by tracking the fluorescent melamine micro-beads with a size of 1 μm.

2.3. Extraction of slip velocity, slip length and local shear rates during shear

The experimental understanding of polymer rheology depends on simple shear rheometric measurements. Usually, rheological properties of polymeric fluids are obtained based on the assumption that a uniform shear field with a constant shear rate ($\dot{\gamma} = V/H$) should prevail across the gap with no slip boundary condition, where V is an imposed (apparent) velocity and H is a sample thickness sandwiched between two parallel plates.

At high shear rates, entangled fluids violate no-slip boundary condition and show strong wall slip during shear. The most effective way to quantify the slip is to introduce the slip length $b = V_s/\dot{\gamma}_b$. The magnitude of b relative to the sample thickness H determines how much the actual bulk shear rate $\dot{\gamma}_b$ is reduced from the apparent rate $\dot{\gamma}$. In this work, the slip velocity V_s and bulk rate $\dot{\gamma}_b$ are directly measured by confocal imaging to estimate the slip length, b, for both solutions. Specifically, to obtain accurate local shear rates, the velocity profiles with high

spatial resolutions were constructed across the gap from PTV. Then, $\dot{\gamma}_b$ was evaluated from the velocity profile using ordinary least squares regression. The formation of two or more flow regimes with different local shear rates under the same imposed rate was defined from the best fits.

3 Results and discussion

3.1. Conventional rheometric measurements

Fig. 3a shows dynamic storage and loss moduli G' and G'' of the two 13 wt% PBD solutions made with 1.5KPBD and 10KPBD respectively. The linear viscoelastic characteristics of these two samples are listed in Table 2, where the plateau modulus G_{pl} was determined from the value of G' at a frequency where G'' shows a minimum, and the longest relaxation time τ is estimated from the inverse of the crossover frequency ω_c where $G' = G''$. The similar value of G_{pl} confirms that the level of chain entanglement is the same in these two PBD solutions. The number of entanglements per chain can be estimated to be around 54 according to $Z = (M_w/M_e)\phi^{1.2}$, where M_w is the molecular weight of the parent PBD, M_e the entanglement molecular weight for PBD melts, taken to be 1600 g mol^{-1}. The Rouse relaxation time of two solutions is determined to be $\tau_R = \tau/3Z$. Given l_{ent} = 3.8 nm,[35] we find a to be *ca.* 15 nm at 13 wt% of 1MPBD.

Table 2 lists $Wi_{ws\text{-}bnl}$ for the two polymer solutions by taking H = 50 μm. According to eqn (2), to observe shear banding in the bulk, we need to apply Wi in excess of either 17 or 240 respectively for the two solutions. By choosing two different solvents, we have estimated b_{max} to differ by a factor of ten as listed in Table 2. Here b_{max} is calculated based on the estimated values of η from Fig. 3.

Next, we performed startup shear experiments to investigate the rheological responses at a narrow gap of H = *ca.* 50 μm in the steady state. Fig. 3b displays the flow curves, showing steady shear stress against the nominal Wi, where the shear rate is given by $\Omega R/H$, with Ω the angular velocity, R the disk radius. The two flow curves are very similar, showing the characteristic of stress plateau, both considerably below the curves of $|G^*|$ *vs.* $\omega\tau$. Because the parallel-disc setup was used to make these measurements, Fig. 3b only reflects an approximate shear stress *vs.* rate relationship.

Table 2 Linear viscoelastic properties and slip characteristics

Sample	G_{pl} (kPa)	τ^a (s)	$Z(\phi)^b$	$\tau_R{}^c$ (s)	η^d (kPa s)	$a(\phi)^e$ (nm)	$b_{max}{}^f$ (mm)	$Wi_{ws\text{-}bnl}{}^g$
1M(13%)1.5K	9.7	36	54	0.22	288	15	6.0	240
1M(13%)10K	9.4	68	54	0.42	395	15	0.4	17

[a] Terminal relaxation times are estimated as $\tau = \omega_c^{-1}$, where ω_c (in rad s^{-1}) is the crossover frequency in a frequency sweep test. [b] Entanglement density, $Z(\phi)$, is calculated by $(M_w/M_e)\phi^{1.2}$, where M_e = 1600 g mol^{-1} for 1,4 PBD melts. [c] Rouse times of two solutions are determined as $\tau_R = \tau/3Z$. [d] The zero shear viscosity of the polymer solutions is estimated from Fig. 3. [e] Interfacial layer thickness of polymer solutions is estimated to be $a(\phi) = l_{ent}\phi^{-0.66}$, where l_{ent} = 3.8 nm for pure PBD melts and ϕ is the polymer volume fraction. [f] The theoretical maximum extrapolation length is estimated to be $b_{max} = (\eta/\eta_s)a(\phi)$, where η_s for 1.5KPBD and 10KPBD is 0.7 and 14 Pa s respectively. [g] The critical Weissenberg number is estimated to be $Wi_{ws\text{-}bnl} = 2b_{max}/H$, where H = 50 μm.

3.2. Homogenous shear in the Newtonian regime (Wi < 1.0)

To check the reliability and performance of our confocal rheoscope, we sheared 1M(13%)1.5K in the terminal regime (Wi < 1.0) where it behaves like a Newtonian liquid. Fig. 4a shows that there is no stress overshoot at a low shear rate $\dot{\gamma}$ = 0.01 s^{-1} (Wi = 0.36). Under this condition, the velocity profile is uniform across the sample thickness at all times, where the bulk shear rate ($\dot{\gamma}_b \sim 0.009$ s^{-1}) is close to the imposed shear rate as shown in Fig. 4b. Small deviation from the imposed shear rate indicates weak wall slip near both top and bottom plates occurs ($V_s \sim 0.03$ μm s^{-1}). These results are consistent

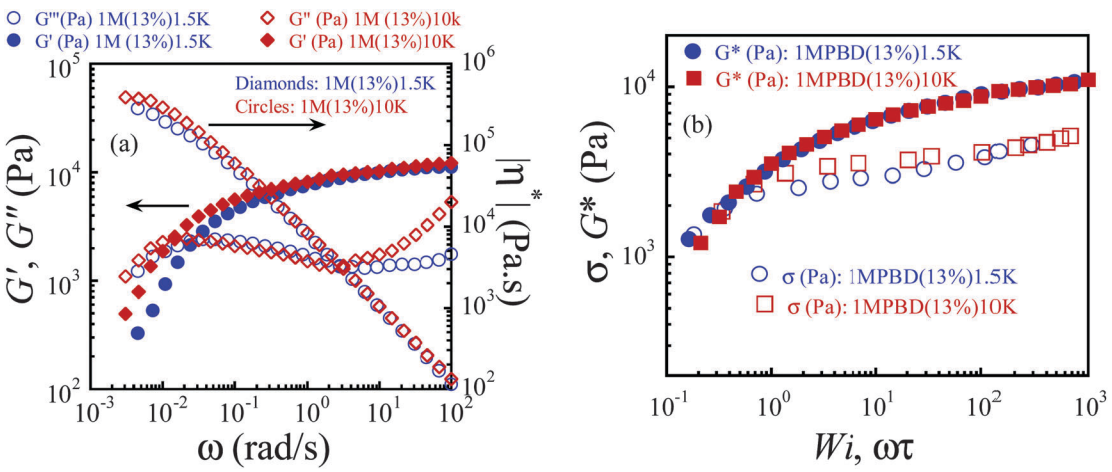

Fig. 3 (a) Small amplitude oscillatory shear (SAOS) measurement of two well-entangled PBD solutions. Dynamic storage, loss moduli and complex viscosity of 1M(13%)1.5K and 1M(13%)10K as a function of frequency using strain amplitude of 5% at room temperature (geometry: a 20 mm parallel-disk cell with separation of 1 mm). (b) Steady shear stress *versus* Wi (geometry: a 20 mm parallel disk with a gap distance of *ca.* 50 μm), along with the oscillatory shear data of G^* *versus* the dimensionless oscillation frequency ($\omega\tau$) for two PBD solutions.

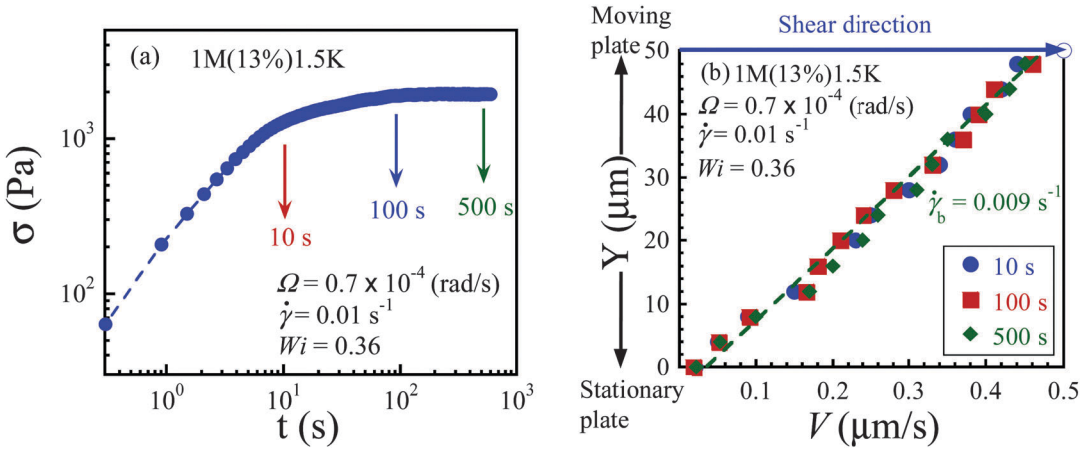

Fig. 4 (a) Shear stress response upon startup shear at a rate of 0.01 s^{-1} as a function of time. The arrows indicate the moments when the velocity profiles were measured and presented in (b). Linear velocity profiles prevail at different times at such a low shear rate (Wi = 0.36), involving the 20 mm-diameter parallel-disk with a separation of 50 μm. The open circle represents the velocity of the upper plate, not PTV measurement.

with previous reports[18,30] of homogenous shear in entangled polymers when Wi < 1.0.

3.3. Strong slip in 1M(13%)1.5K solution (1.0 < Wi ≤ 288)

At a shear rate of 0.4 s^{-1} (Wi ~ 14), the shear stress overshoot occurred during startup shear as shown in Fig. 5a, and the velocity profile is linear around t = 1 s before stress overshoot and displays strong slip after the stress maximum as shown in Fig. 5b. The velocimetric measurement reveals that the bulk of the sample experiences a mere shear rate of 0.03 s^{-1}, which is comparable to the reciprocal of the terminal relaxation time (τ = 36 s). At higher shear rates of 1.6, 3.0 and 8.0 s^{-1} (Wi = 57–288), apparent wall slip appears to be the only form of shear inhomogeneity near the steady state as shown in Fig. 6a and b. Accessing higher deformation rates (Wi > 296) to observe bulk shear banding across the gap is infeasible for PBD1M(13%)1.5K because our PTV technique is limited to shear rates up to 10 s^{-1}.

3.4. Shear banding in 1M(13%)10K (100 ≤ Wi ≤ 408)

The intrinsic ability to undergo wall slip can be considerably reduced by using a polymeric solvent with a sufficiently high molecular weight to increase the upper bound for the interfacial viscosity η_i.[29] In this section, we only focus on steady-state velocity profiles at different shear rates in the stress plateau region. At a low shear rate $\dot{\gamma}$ = 0.3 s^{-1} (Wi ~ 20), this solution also violates the no-slip boundary condition at the top and bottom plates after stress maximum is reached, and strong slip prevails across the gap as shown in Fig. 7a and b. On the other hand, when Wi > 100, shear banding emerges across the small gap. The growth of shear stress for shear rates of 1.5, 3.0 and 6.0 s^{-1} during startup shear is plotted in Fig. 8a. Fig. 8b shows that the velocity profile becomes nonlinear, characteristic of shear banding (with three different local shear rates of 0.15, 0.86 and 4.39 s^{-1}) in the steady state for a nominal shear rate of 1.5 s^{-1}. Previous velocimetric measurements on polymer

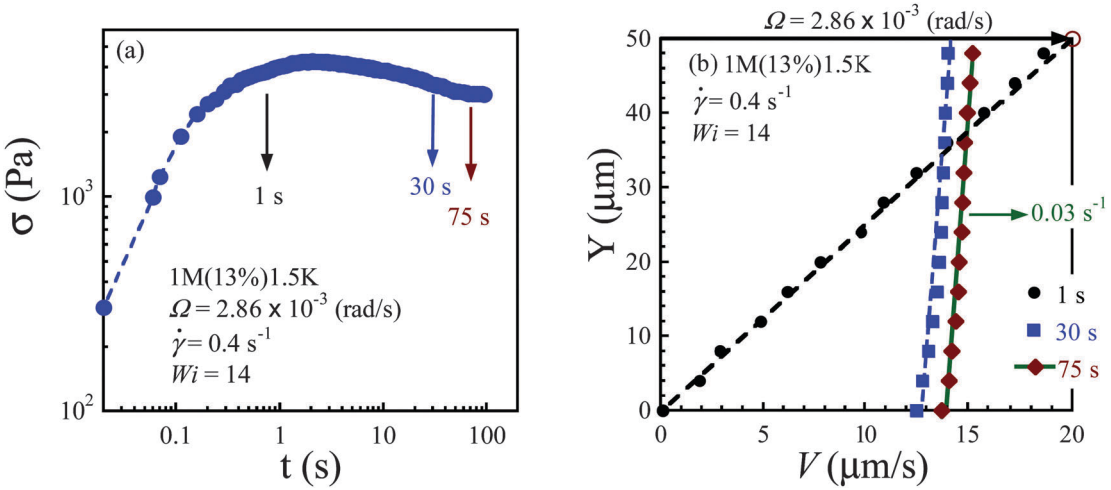

Fig. 5 (a) Shear stress response upon startup shear at a rate of 0.4 s^{-1} (Wi = 14) for 1M(13%)1.5K. (b) The evolution of the velocity profile at different times (t = 1, 30 and 75 s). Velocity profile is linear across the gap, before stress maximum then massive slip developed at long times, in the 20 mm-diameter parallel-disk shear cell with a separation of 50 μm. The open circle represents the velocity of the upper plate, not PTV measurement.

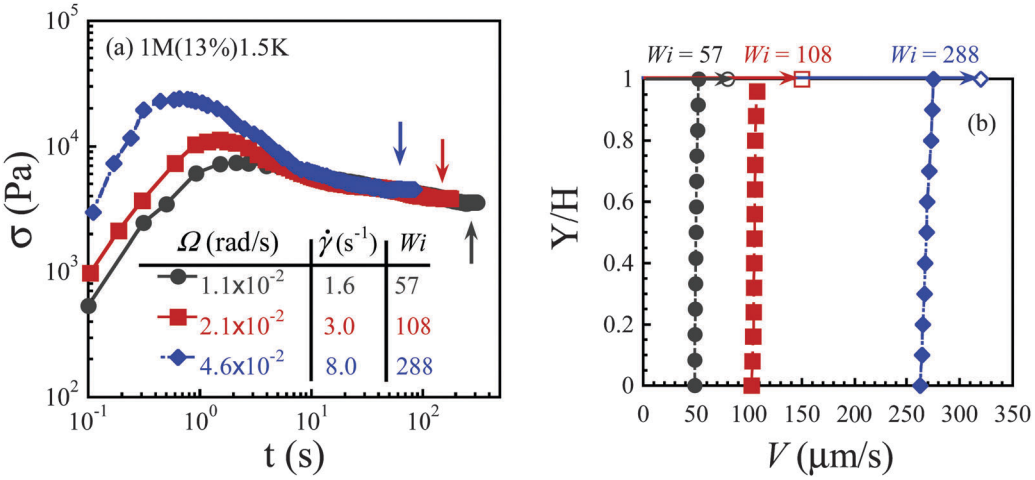

Fig. 6 (a) Shear stress response upon startup shear at different shear rates ($\dot{\gamma}$: 1.6, 3.0 and 8.0 s^{-1}) for 1M(13%)1.5K. (b) The linear velocity profiles in the bulk with strong slip at both surfaces at the moments indicated by the vertical arrows in (a), from the 20 mm-diameter parallel-disk shear cell with a separation of 50 μm (at $\dot{\gamma}$ = 1.6 and 3.0 s^{-1}) and 40 μm (at $\dot{\gamma}$ = 8.0 s^{-1}). The rheometric velocities of upper plates are represented by open symbols.

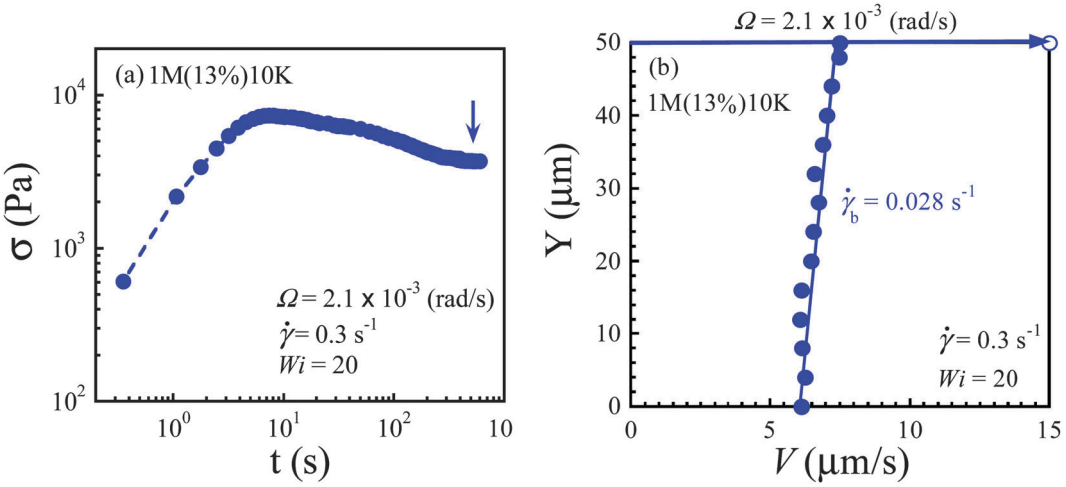

Fig. 7 (a) Shear stress response upon startup shear at a rate of 0.3 s^{-1} (Wi = 20). (b) Steady-state linear velocity profile with apparent wall slip for 1M(13%)10K when Wi < Wi$_{ws\text{-}bnl}$, obtained from the 20 mm-diameter parallel-disk shear cell with a separation of 50 μm. The open circle represents the velocity of the upper plate, not PTV measurement.

solutions[14] have also reported the existence of multiple shear banding across the gap. For shear rates of 3.0 and 6.0 s^{-1}, permanent shear banding persists across the gap even after hundreds of strain units, as shown in Fig. 8c. Accompanying the high shear band is also significant wall slip. For apparent shear rates of 1.5, 3.0 and 6.0 s^{-1}, the local rate in the high shear band is 4.39, 5.67 and 14.48 s^{-1} respectively. As a function of the apparent shear rate, the local shear rate varies in each of the low, medium or high band, as shown in Fig. 8d. The local shear rate in the high band seems to increase exponentially with an apparent shear rate.

3.5. Normalized steady state velocity profiles: slip *vs.* shear banding

Fig. 9a and b respectively present the normalized steady-state velocity profiles for the two solutions at different Wi. In Fig. 9a, the 1M(13%)1.5K solution shows nothing else but massive slip in the range of Wi from 14 to 288. In contrast, Fig. 9b shows that bulk shear banding develops across the gap in the range of Wi from 102 to 408 for 1M(13%)10K. Fig. 9c displays the steady state velocity profiles at comparable Wi = 288 and 272; $\dot{\gamma}\tau_R$ = 1.8 and 1.7, showing slip and bulk shear banding respectively of the two solutions.

Our PTV measurements allow us to examine how the wall slip grows in magnitude, *i.e.*, how the slip velocity V_s increases with the applied rate $\dot{\gamma}$ toward its maximum. According to $V = 2V_s + \dot{\gamma}_b H$, V_s would change linearly with Wi as

$$\mathrm{Wi} = (V/H)\tau = 2V_s/(H/\tau) + \tau\dot{\gamma}_b$$

if the bulk rate $\dot{\gamma}_b$ were to remain little changed with Wi. Fig. 9d plots V_s against Wi for both PBD solutions. With increasing Wi, the value of V_s grows linearly for 1M(13%)1.5K. Similar behavior

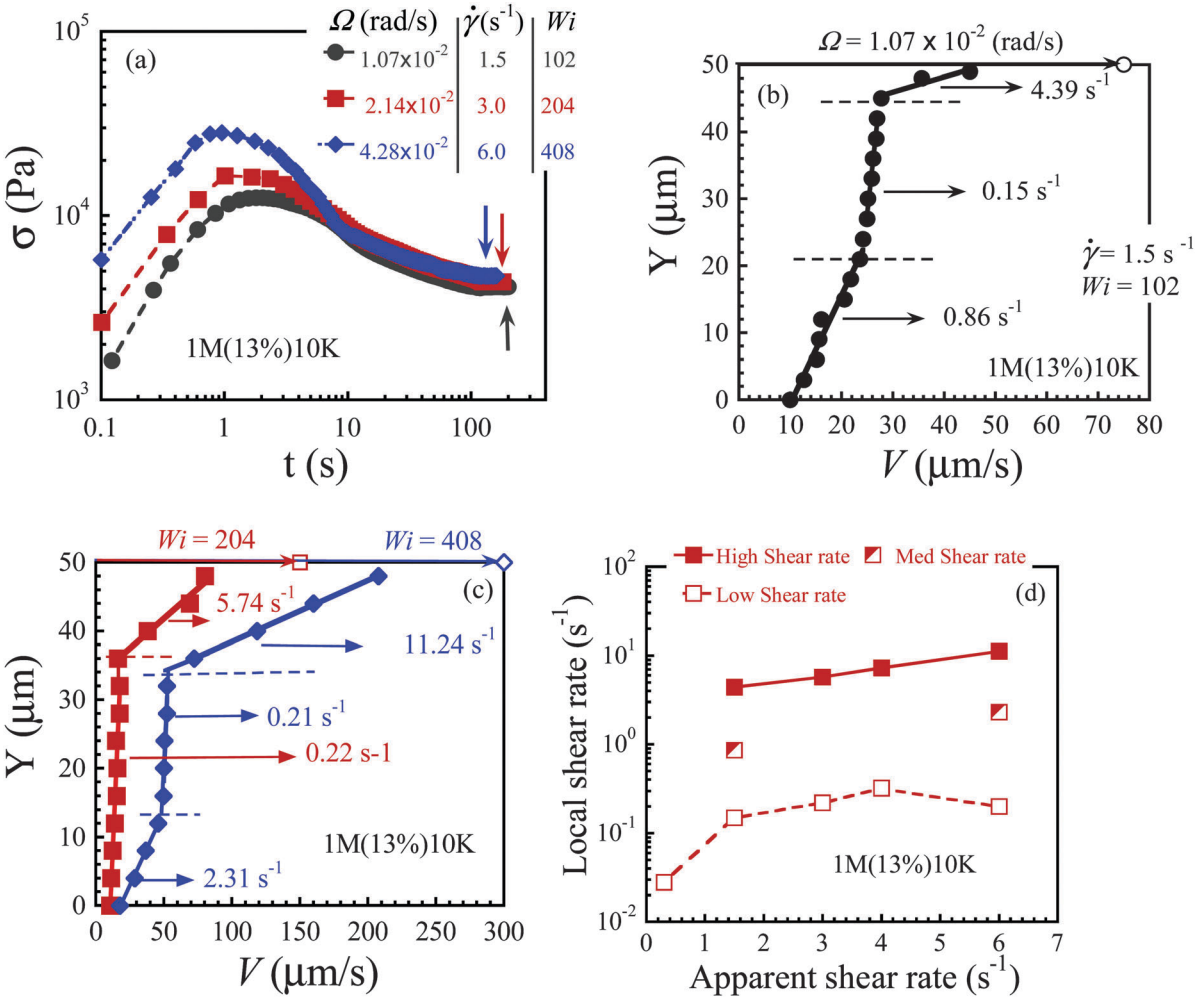

Fig. 8 (a) Shear stress response upon startup shear at different shear rates ($\dot{\gamma}$: 1.5, 3.0 and 6.0 s^{-1}) for 1M(13%)10K measured from the 20 mm-diameter parallel-disk shear cell with a separation of 50 μm. (b) Shear banded velocity profile with formation of three flow regimes (0.15, 0.86 and 4.39 s^{-1}) for an apparent shear rate of 1.5 s^{-1} in the steady state as indicated by the vertical arrow in (a). (c) Banded velocity profiles of 3.0 and 6.0 s^{-1} in the steady state as indicated by the vertical arrow in (a). The rheometric velocities of upper plates are represented by open symbols in (b and c). (d) The local shear rates (obtained from PTV measurements) *versus* apparent shear rates for 1M(13%)10K.

is also observed for 1M(13%)10K up to 1.0 < Wi < 20. The slip velocity V_s starts to deviate from the linearity for Wi > 20, confirming that the shear rate $\dot{\gamma}_b$ remained unchanged up to Wi = 20. The value V_s of 1M(13%)10K stays well below that of 1M(13%)1.5K for all values of Wi – noting the different scales used for the double-*Y* axes. When the increase of V_s starts to deviate downward from linear growth with Wi, it has already reached its maximum at 6 μm s^{-1}, which coincides with the theoretical estimate of eqn (3): $V_{s(max)} \sim b_{max}/\tau = 420/68 = 6.2$ μm s^{-1}. Because of the poor spatial resolution, the higher value of V_s observed at high Wi indicates apparent wall slip that involves a slip layer increasingly thicker than one monolayer. Fig. 9e shows the changes in the slip length $b = V_s/\dot{\gamma}_b$ as a function of Wi for the two solutions. The slip length b ranges from 10 to ~1100 μm for 1M(13%)1.5K, which is one order of magnitude higher than slip length of 1M(13%)10K (maximum $b \sim 190$ μm). This can be estimated from the information in Table 1 showing that η_s of PBD10K is 20 times as high as that of 1.5KPBD.

3.6. Relationship between local and apparent Wi and comparison with previous work

Upon extracting the local, *i.e.*, bulk, Weissenberg numbers from our velocimetric measurements, we show the relationship between the bulk Weissenberg number Wi_b and nominal Wi in Fig. 10. Here we compare our findings with the previous work obtained in a narrow-gap to address and discuss why only either linear velocity profile or wall slip was observed in the previous report. Hayes and coworkers[30] studied five different entangled solutions with different volume fractions ϕ based on two high molar mass PBD ($M_w = 0.7 \times 10^6$ g mol^{-1}, $M_w/M_n = 1.1$) and PBD ($M_w = 0.2 \times 10^6$ g mol^{-1}, $M_w/M_n = 1.05$) in an un-entangled PBD1K solvent ($M_w = 1 \times 10^3$ g mol^{-1}). These PBD solutions with a wide range of level of entanglements ($8 \leq Z \leq 56$) were reported to show a linear velocity profile with some wall slip. We estimate the rheological properties and slip characteristics of five solutions as shown in Table 3. Among these five solutions, 0.2M(40%)1K, 0.2M(60%)1K and 0.7M(20%)1K

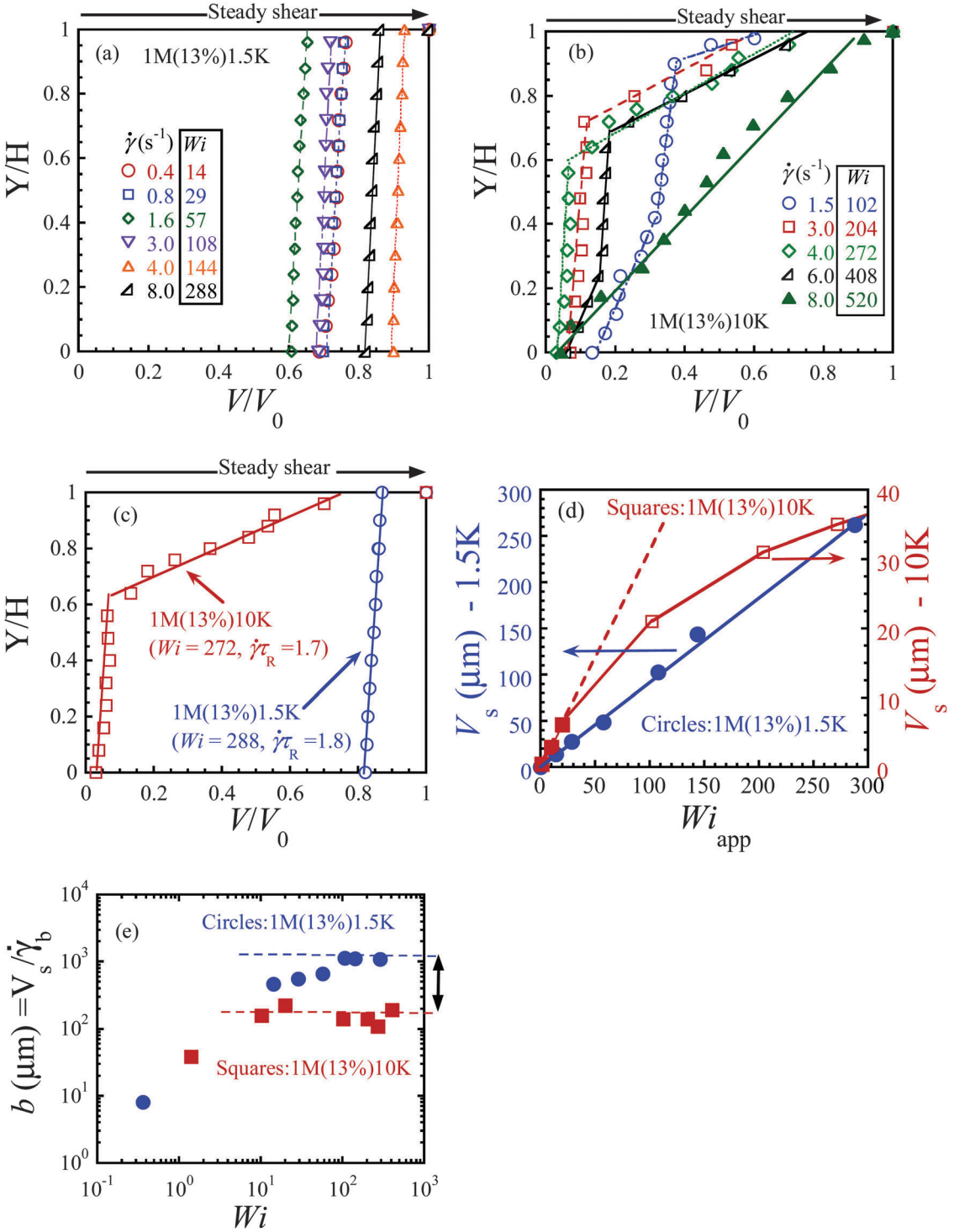

Fig. 9 Snap shots of velocity profiles in the steady state for (a) 1M(13%)1.5K (slip-like behavior) and (b) 1M(13%)10K (bulk shear banding at 100 ≤ Wi ≤ 408 and uniform shear at Wi = 520). (c) The normalized velocity profiles of the two PBD solutions at Wi = 288 and 272; $\dot{\gamma}\tau_R$ = 1.8 and 1.7, showing slip and shear banding respectively. (d) Slip velocity *versus* apparent Wi for the two PBD solutions. (e) Estimated slip length, *b*, *versus* apparent Wi for the two PBD solutions where the vertical bar indicates the maximum difference.

have a sufficiently high level of entanglements ($32 \leq Z \leq 56$) capable of producing shear banding across the gap at high values of Wi. We also note that only 0.7M(20%)1K was sheared at sufficiently high Wi ($9 \leq$ Wi ≤ 114). The two PBD solutions, based on the parent PBD200K named 0.2M(40%)1K and 0.2M(60%)1K, were only explored in the Newtonian regime ($0.08 \leq$ Wi ≤ 0.7). It is well established that a linear velocity profile should be maintained across the gap when Wi < 1.0.[18,29]

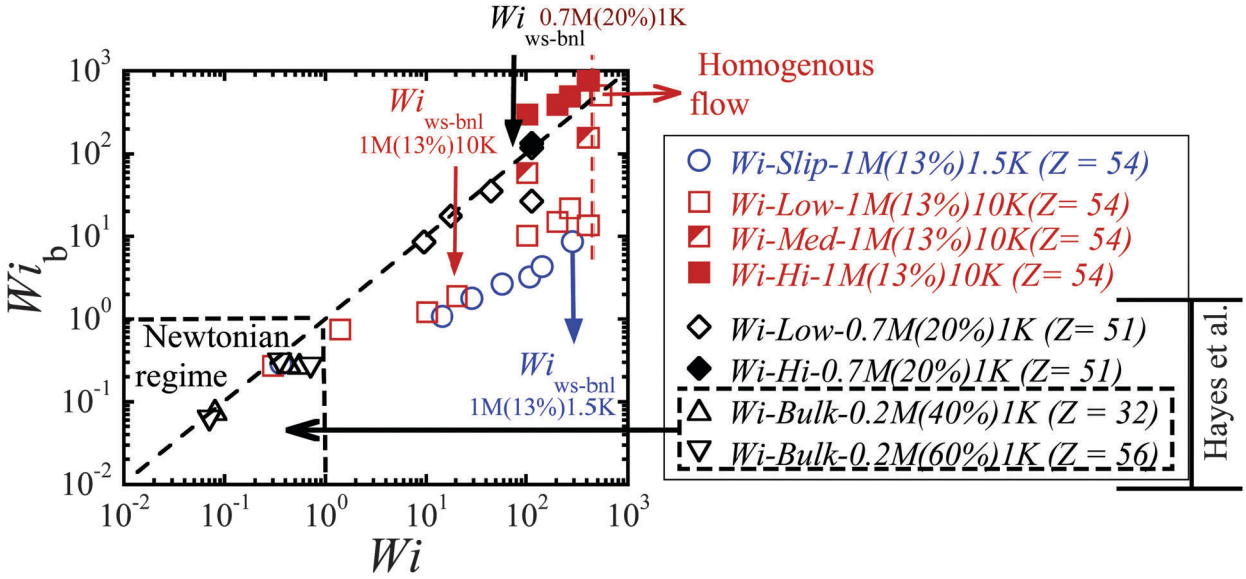

Fig. 10 Local Wi_b against apparent Wi for five PBD solutions with a sufficiently high level of entanglements ($32 \leq Z \leq 56$). Diamonds and triangles are extracted from the work of Hayes *et al.* Both 0.2M(40%)1K and 0.2M(60%) were only sheared at a low shear rate such that $Wi < 1.0$ (highlighted by the dashed box in the Newtonian regime). At high $Wi > 100$, the coexistence of high and low Wi_b appears across the micron scale gap for 1M(13%)10K, in contrast with apparent slip of 1M(13%)1.5K that keeps Wi_b low as indicated by the circles. For 0.7M(20%)1K, the coexistence of a high and a low shear band has been reported by Hayes *et al.* at Wi = 113. Note that values of $Wi_{ws\text{-}bnl}$ for 1M(13%)1.5K, 1M(13%)10K, and 0.7M(20%) are highlighted by vertical blue, red and black arrows respectively.

Table 3 Composition and linear rheological properties of PBD solutions reported in the work of Hayes *et al.*[30]

Sample	G_{pl}[a] (kPa)	τ (s)	$Z(\phi)$	$\eta(\phi)$[d] (kPa s)	$a(\phi)$ (nm)	$b_{max} = (\eta/\eta_s)a(\phi)$[e] (mm)	$Wi_{ws\text{-}bnl} \sim 2b_{max}/H$[f]
0.7M(5%)1K	1.3	2.7	12[b], 8[c]	3	27	0.02	0.5
0.7M(10%)1K	7.5	11	27[b], 20[c]	67	17	0.26	7
0.7M(20%)1K	44	31.6	63[b], 51[c]	1142	11	2.82	80
0.2M(40%)1K	220	0.8	41[b], 32[c]	145	7	0.25	7
0.2M(60%)1K	511	1	68[b], 56[c]	420	5	0.56	16

[a] Plateau modulus of PBD samples was provided in PhD thesis of Keesha Hayes.[36] [b] $Z(\phi)$ is estimated by $(M_w/M_e)\phi^{1.2}$, where $M_e = 1600$ g mol^{-1} for 1,4 PBD melts. [c] $Z(\phi)$ is reported by Hayes *et al.*, where M_e is assumed to be around 2000 g mol^{-1}. [d] Bulk shear viscosity of polymer solutions is estimated to be $\eta = \frac{\pi^2}{12}G_{pl}\tau$.[5] [e] Maximum extrapolation length is estimated, where solvent viscosity (PBD1K, $M_n \sim 1000$ g mol^{-1}, Aldrich Inc.) is assumed to be around 4.0 Pas at room temperature.[37] The vinyl content of PBD1K (Aldrich 200417) is higher than PBD1.5K (Aldrich 200484) leading to lower T_g and higher viscosity. [f] $Wi_{ws\text{-}bnl}$ is estimated, where $H = 35$ μm.

In general, at low shear rates ($Wi < 1.0$), the nominal and local Weissenberg numbers are the same, which is consistent with previous reports on entangled systems.[18,30] Besides, at Wi = 0.7 and 0.5 (closer to Wi = 1), both 0.2M(40%)1K and 0.2M(60%)1K suffered from some degree of wall slip,[30] as denoted by the triangles in Fig. 10. This is expected.

At higher Wi in the non-Newtonian regime ($Wi > 1.0$), we see that Wi_b remains the order of unity because of the dominant wall slip in 1M(13%)1.5K, except for last two points. In the explored range of apparent shear rates, the solution based on the 1.5 K solvent has b equal to 1100 μm and shows interfacial slip or apparent wall slip only up to Wi = 288 ($\dot{\gamma}\tau_R \sim 1.8$). The PBD solution with a PBD10K solvent shows the coexistence of high and low shear bands, along with wall slip because its $b = 190$ μm. We note that beyond Wi = 100; $\dot{\gamma}\tau_R \sim 0.6$, there can be three bands of different local rates in the bulk for 1M(13%)10K. In contrast, a linear velocity profile without wall slip was reported by Hayes *et al.* for their 0.7M(20%)1K ($Z \sim 51$) till Wi = 45. The lack of wall slip is at odds with their report of wall slip for the other solutions and in disagreement with our findings shown in Fig. 10. When Wi is increased to 113, the velocity profile began to deviate significantly from nominal Wi, displaying shear banding. This response can be consistent with our observation of shear banding, because shear banding should occur for 0.7M(20%)1K when $Wi > Wi_{ws\text{-}bnl} \sim 80$ (see diamonds in Fig. 10). However, Hayes *et al.* suggested that this behavior could be originated from secondary flows due to chain stretching and normal stresses at a high shear rate. Since most of the reported values of Wi in Hayes *et al.*'s measurements are less than critical $Wi_{ws\text{-}bnl}$, except for one date point of 0.7M(20%)1K (at Wi = 113), it is expected to observe a linear velocity profile in their measurements. In this work since the point of PTV observation is so far away from the edge, it is implausible for our results to have anything to do with any edge instability. Thus we have proposed localized chain disentanglement as the origin of shear banding, more systematic studies are required to look for

evidence of the secondary flow phenomenon and the effect of edge failure on the bulk velocity profile of well-entangled PBD solutions in such small-gap shear cells.

3.7. Suppression of edge effects at a small gap

Edge fracture occurs frequently in well-entangled polymeric systems at high Wi in a conventional rheometric setup (with a gap size of 1 mm).[38,39] This phenomenon is attributed to the build-up of normal stresses.[38,40] When edge fracture occurs, the sample may "leak out" at the meniscus during shear leading to a reduced stress response. It has been reported in the literature that a large decrease of the gap distance can minimize the edge effects during shear of entangled polymer solutions.[30] We carry out SAOS to verify whether there is any sample loss during shear banding. Fig. 11 shows that dynamic oscillatory shear data are identical before and after shearing at shear rates of 1.5, 3.0 and 6.0 s^{-1}.

Additionally, it is known that edge fracture would be more severe at high Wi, due to increased normal force. Fig. 12 shows that at higher Wi, a linear velocity profile is actually recovered in the steady state. Specifically, at a sufficiently high shear rate of 8.0 s^{-1}, the uniform shear is recovered (at t = 77 s) after showing transient inhomogeneity (at t = 7.7 s) across the gap. Therefore, we can conclude that edge fracture has been minimized and sample loss is negligible in our measurements, and our setup can be ideal for studying the non-linear response in entangled polymers at high Wi.

3.8. The phase diagram

We can construct a "phase diagram" to summarize our findings in terms of Wi *versus* $2b_{max}/H$, as shown in Fig. 13. Clearly, b_{max} is one of the key parameters to highlight when and what type of shear inhomogeneity may occur at different Wi for a fixed gap. For both 0.7M(20%)1K and 1.0M(13%)1.5K, much higher Wi is required to obtain shear banding, due to a high value of slip length. We should emphasize that this phase diagram can only qualitatively describe whether shear banding occurs or not during shear for well-entangled systems ($Z > 40$).

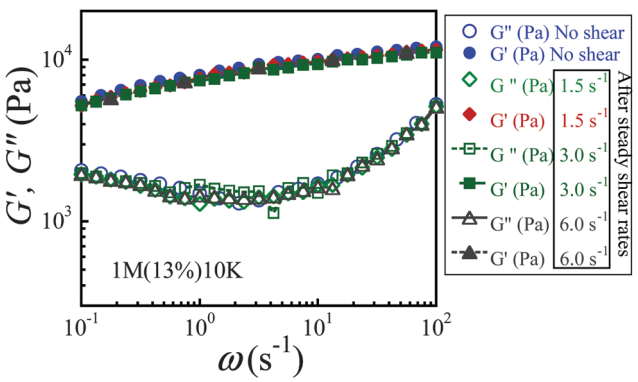

Fig. 11 Small amplitude oscillatory shear (SAOS) measurements before and after shear rates (with 650 s rest time for entanglement recovery after applying steady shear rates). Dynamic storage (closed symbols) and loss (open symbols) moduli of 1M(13%)10K as a function of frequency using strain amplitude of 5% at room temperature.

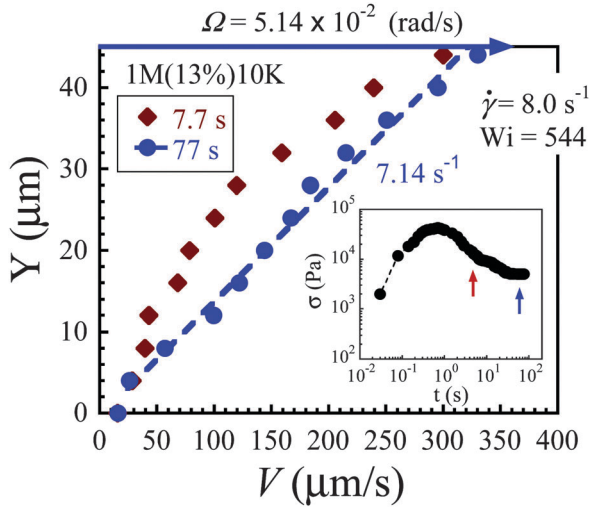

Fig. 12 Restoration of the uniform velocity profile at a high shear rate. Characterization of the velocity profile at high shear rates = 8.0 s^{-1} (Wi = 544) at t = 7.7 and 77 s. The inset shows a shear stress response upon startup shear at a rate of 8.0 s^{-1}.

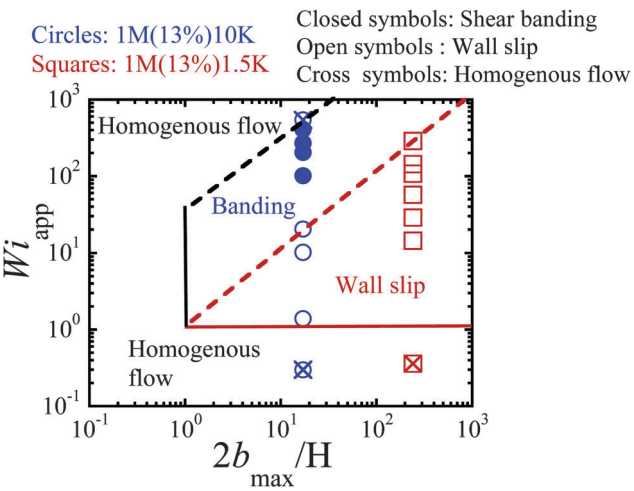

Fig. 13 Phase diagram in the parameter space of apparent Wi *versus* $2b_{max}/H$ for our findings at a small gap for PBD solutions (Z = 54) in different PBD solvents.

4 Conclusions

In this study, two entangled PBD solutions with the same level of entanglement (Z = 54) have been subjected to various values of nominal shear rate $\dot{\gamma}$ to explore their nonlinear rheological responses in a shear cell with a small gap distance in the 50 micron range. Because the gap distance was unconventionally small, the PTV observations could be free of edge effects without implementation of a cone-partitioned plate.[39,41–43] Using a confocal microscope integrated with a rotational rheometer, we obtain simultaneous global rheology (apparent rheometric measurements) and local velocity profiles. This setup allows us to probe when and what type of shear inhomogeneity (interfacial slip *vs.* shear banding) occurs across the gap. For the entangled PBD solution made with a low molecular weight PBD (M_w = 1.5 kg mol^{-1}), only interfacial slip or

apparent wall slip can be observed up to a shear rate of 8 s^{-1}. In contrast, the second solution, the higher molecular weight PBD (M_w = 10 kg mol^{-1}) solvent reduces the magnitude of the slip length b so that apart from wall slip bulk shear banding can also take place at the experimentally accessible shear rates. The prevalence of interfacial slip in 1M(13%)1.5K is consistent with the findings of Hayes and coworkers.[30,31] On the other hand, 1M(13%)10K exhibits shear banding despite a small gap distance of 50 μm, when imposed Wi exceeds a critical value if Wi, *i.e.*, $2b_{max}/H$. Finally, at sufficiently high Wi, shear homogeneity is restored across the gap for 1M(13%)10K.

Acknowledgements

This study was supported by the European Research Council under the European Unions Seventh Framework Programme (FP/2007-2013)/ERC Grant, agreement no. 337820 (to P.E.B) and NSF-DMR-1105135 (to S.Q.W). We would like to thank Malvern Instruments Ltd for loaning the rheometer. We are grateful to Michiel Kreutzer, and Yogesh Harshe for fruitful discussion.

Notes and reference

1 M. Rubinstein and R. Colby, *Polymer Physics*, Oxford, 2000.
2 R. B. Bird, R. C. Armstrong and O. Hassager, *Dynamics of polymer liquids*, Wiley, New York, 1977.
3 J. D. Ferry, *Viscoelastic Properties of Polymers*, Wiley, New York, 1980.
4 P. G. deGennes, *J. Chem. Phys.*, 1971, **55**, 572–579.
5 M. Doi and S. F. Edwards, *The theory of polymer dynamics*, Oxford University, Oxford, 1986.
6 T. C. B. McLeish, *Adv. Phys.*, 2002, **5**, 1379–1527.
7 S. Q. Wang, S. Rvindranath, Y. Wang and P. E. Boukany, *J. Chem. Phys.*, 2007, **127**, 064903.
8 (*a*) N. A. Spenely, M. E. Cates and T. C. B. McLeish, *Phys. Rev. Lett.*, 1993, **71**, 939–942; (*b*) M. Britton and P. Callaghan, *Phys. Rev. Lett.*, 1997, **78**, 4930; (*c*) R. W. Mair and P. T. Callaghan, *Europhys. Lett.*, 1996, **36**, 719; (*d*) M. M. Britton, R. W. Mair, R. K. Lambert and P. T. Callaghan, *J. Rheol.*, 1999, **43**, 897.
9 Y. T. Hu and A. Lips, *J. Rheol.*, 2005, **49**, 1001–1027.
10 P. E. Boukany and S.-Q. Wang, *Macromolecules*, 2008, **41**, 1455–1464.
11 M. A. Fardin, T. Divoux, M. A. Guedeau-Boudeville, I. Buchet-Maulien, J. Browaeys, G. H. McKinley, S. Mannevillece and S. Lerouge, *Soft Matter*, 2012, **8**, 2535–2553.
12 (*a*) J. B. Salmon, A. Colin, S. Manneville and F. Molino, *Phys. Rev. Lett.*, 2003, **90**, 228303; (*b*) S. Manneville, A. Colin, G. Waton and F. Schosseler, *Phys. Rev. E: Stat., Nonlinear, Soft Matter Phys.*, 2007, **75**, 061502; (*c*) P. Lettinga and S. Manneville, *Phys. Rev. Lett.*, 2009, **103**, 24830.
13 (*a*) P. Tapadia and S.-Q. Wang, *Phys. Rev. Lett.*, 2006, **96**, 016001; (*b*) P. E. Boukany and S. Q. Wang, *J. Rheol.*, 2007, **51**, 217; (*c*) S. Ravindranath and S. Q. Wang, *J. Rheol.*, 2008, **52**, 957.
14 S. Ravindranath, S.-Q. Wang, M. Olechnowicz and R. P. Quirk, *Macromolecules*, 2008, **41**, 2663–2670.
15 Y. T. Hu, *J. Rheol.*, 2010, **54**, 1307–1323.
16 P. T. Callaghan and A. M. Gil, *Macromolecules*, 2000, **33**, 4116–4124.
17 S. Jaradat, M. Harveyab and T. A. Waigh, *Soft Matter*, 2012, **8**, 11677–11686.
18 P. E. Boukany, Y. T. Hu and S.-Q. Wang, *Macromolecules*, 2008, **41**, 2644–2650.
19 P. E. Boukany and S.-Q. Wang, *Soft Matter*, 2009, **5**, 780–789.
20 P. E. Boukany and S.-Q. Wang, *J. Rheol.*, 2009, **53**, 73–83.
21 I. Kunita, K. Sato, Y. Tanaka, Y. Takikawa, H. Orihara and T. Nakagaki, *Phys. Rev. Lett.*, 2012, **109**, 248303.
22 P. E. Boukany, S.-Q. Wang and X. Wang, *Macromolecules*, 2009, **42**, 6261–6269.
23 Y. Fang, G. Wang, N. Tian, X. Wang, X. Zhu, P. Lin, G. Ma and L. Li, *J. Rheol.*, 2011, **55**, 939–949.
24 P. E. Boukany and S.-Q. Wang, *Macromolecules*, 2010, **43**, 6950–6952.
25 S. Cheng and S.-Q. Wang, *J. Rheol.*, 2012, **56**, 1413–1428.
26 Y. Li, M. Hu, G. B. McKenna, C. J. Dimitriou, G. H. McKinley, R. M. Mick, D. C. Venerus and L. A. Archer, *J. Rheol.*, 2013, **57**, 1411–1428.
27 S.-Q. Wang, G. Liu, S. Cheng, P. E. Boukany, Y. Wang and X. Li, *J. Rheol.*, 2014, **58**, 1059–1069.
28 S. Ravindranath, S.-Q. Wang, M. Olechnowicz, V. S. Chavan and R. P. Quirk, *Rheol. Acta*, 2011, **50**, 97–105.
29 S.-Q. Wang, S. Ravindranath and P. E. Boukany, *Macromolecules*, 2011, **44**, 183–190.
30 K. A. Hayes, M. R. Buckley, I. Cohen and L. A. Archer, *Phys. Rev. Lett.*, 2008, **101**, 218301.
31 K. A. Hayes, M. R. Buckley, H. Qi, I. Cohen and L. A. Archer, *Macromolecules*, 2010, **43**, 4412–4417.
32 (*a*) L. Leger, E. Raphael and H. Hervet, *Adv. Polym. Sci.*, 1999, **138**, 185–225; (*b*) M. M. Denn, *Annu. Rev. Fluid Mech.*, 2001, **33**, 265; (*c*) E. Granick, *et al.*, *J. Polym. Sci., Part B: Polym. Phys.*, 2003, **41**, 2755; (*d*) G. S. Hatzikiriakos, *Prog. Polym. Sci.*, 2012, **37**, 624.
33 P. E. Boukany and S.-Q. Wang, *Macromolecules*, 2009, **42**, 2222–2228.
34 P. E. Boukany, O. Hemminger, S.-Q. Wang and L. J. Lee, *Phys. Rev. Lett.*, 2010, **105**, 027802.
35 L. J. Fetters, D. J. Lohse, D. Richter, T. A. Witten and A. Zirkel, *Macromolecules*, 1994, **27**, 4639–4647.
36 K. Hayes, *Nonlinear Rheolgy of Entangled Polymers: Implications of Shear Banding and Interfacial Slip*, PhD dissertation, Cornell University, 2009.
37 P. Tapadia, PhD thesis, University of Akron, 2005.
38 R. G. Larson, *Rheol. Acta*, 1992, **31**, 213–263.
39 S. Ravindranath and S. Q. Wang, *J. Rheol.*, 2008, **52**, 957–980.
40 R. I. Tanner and M. Keentok, *J. Rheol.*, 1983, **27**, 47–57.
41 J. Meissner, R. W. Garbella and J. Hostettler, *J. Rheol.*, 1989, **33**, 843–864.
42 T. Schweizer, *Rheol. Acta*, 2002, **41**, 337–344.
43 F. Snijkers and D. Vlassopoulos, *J. Rheol.*, 2011, **55**, 1167–1186.